Numerical Predictions of In-Cylinder Phenomenon in Methanol Fueled Locomotive Engine Using High Pressure Direct Injection Technique

Conference Paper · April 2021

DOI: 10.4271/2021-01-0492

CITATIONS
6

READS
68

3 authors, including:

Dhananjay Kumar
Indian Institute of Technology Kanpur
21 PUBLICATIONS **56** CITATIONS

SEE PROFILE

Avinash Kumar Agarwal
Indian Institute of Technology Kanpur
517 PUBLICATIONS **16,299** CITATIONS

SEE PROFILE

2021-01-0492 Published 06 Apr 2021

Numerical Predictions of In-Cylinder Phenomenon in Methanol Fueled Locomotive Engine Using High Pressure Direct Injection Technique

Dhananjay Kumar, Hardikk Valera, and Avinash Kumar Agarwal IIT Kanpur

Citation: Kumar, D., Valera, H., and Agarwal, A.K., "Numerical Predictions of In-Cylinder Phenomenon in Methanol Fueled Locomotive Engine Using High Pressure Direct Injection Technique," SAE Technical Paper 2021-01-0492, 2021, doi:10.4271/2021-01-0492.

Abstract

Petroleum products are used to power internal combustion engines (ICEs). Emissions and depletion of petroleum reserves are important questions that need to be answered to ensure existence of ICEs. Indian Railways (IR) operates diesel locomotives, which emit large volume of pollutants into the environment. IR is looking for an alternative to diesel for powering the Locomotives. Methanol has emerged as a replacement for petroleum fuels because it can be produced from renewable resources as well as from non-renewable resources in large quantities on a commercially viable scale. It has similar/superior physico-chemical properties, which reduce tailpipe emissions significantly. It is therefore necessary to understand the in-cylinder phenomenon in methanol fueled engines before its implementation on a large-scale. In this study, efforts have been made to understand the in-cylinder phenomenon in large-bore locomotive engines using CFD tools. 3-D model was prepared and validated using the experimental data of the baseline diesel. Afterward, this validated model was modified for 90% diesel replacement (on energy basis) by methanol in the engine by employing high pressure direct injection (HPDI) technique via a co-axial injector. Pilot diesel injection was used to ignite the methanol-air mixture. Optimized dimensions of co-axial injector obtained from 1-D simulation were used as primary inputs to the 3-D model. This study provided insights into complex combustion phenomenon of methanol-fueled locomotive engine using HPDI technique. 3-D model was used to understand spatial and temporal variations of different combustion parameters such as in-cylinder pressure variations, temperature variations, fuel-air mixing processes, etc. From the simulation study, it was concluded that locomotive engine fueled with methanol and pilot diesel shows more homogeneous fuel-air mixture compared to only diesel fueling. Also, the maximum in-cylinder temperature for methanol fueled locomotive was found significantly lesser vis-à-vis diesel-fueled which led to lesser NOx formation.

Introduction

Limited fuel resources and increased concerns of environmental preservation have drawn global attention for exploring the use of alternative fuels. Alternative fuels for ICEs are one of the practical approaches to tackle galloping global energy demands and reducing tailpipe emissions simultaneously [1-2]. Among various alternative fuels, oxygenated fuels such as alcohols, esters, and ethers have been investigated and seem to offer great potential in reducing engine-out emissions [3-8]. Among them, methanol has gained strong attention in Asian countries such as China, India, etc. because these countries possess abundant raw feedstock resources for methanol production such as low-value biomass, high ash coal, natural gas, and municipal solid waste (MSW) [9-14].

Methanol is a single carbon fuel (CH_3OH). It has ~ 50% (w/w) inherent oxygen in its molecular structure, which leads to a significant reduction in CO due to CO - CO_2 conversion. Simultaneously, it reduces Smoke, Soot, or Particulate matter (SSP), by avoiding the formation of rich-mixture zones during combustion [15] and NO_X emissions [16-20]. It has a relatively high heat of vaporization and flame speed [21]. The high latent heat of vaporization delivers higher cooling effects, which leads to relatively high brake thermal efficiency. However, this further alleviates the cold start issue during low atmospheric conditions. Since methanol does not contain any sulfur, its utilization in engines does not produce sulfur dioxide (SO_2) and sulfur trioxide (SO_3). Economically methanol is cheaper compared to diesel. However, lower cetane number and viscosity limit its usage in diesel engines without substantial modification.

Applications such as manufacturing, material processing, mining, military, new generation agriculture equipment, vehicles, ships, and locomotives generally use conventional diesel engines. Diesel engine market revenue is forecasted to grow at a CAGR of 3% during 2019-2025 [22]. Therefore, investigations for methanol usage in conventional diesel engines have become important for transportation industry. In India, heavy-duty vehicles mostly use diesel as primary fuels. As per statistics of FY-2015 70, 20 and 10% of diesel engine shares were for commercial, industrial, and residential usage, respectively [23]. Indian Railway (IR) is a prime mover of the Indian

economy, which uses diesel locomotives for traction. Emissions from diesel locomotives although generated by heterogeneous combustion, have become one of the major sources of environmental pollution. Rapid electrification of rail-road sector and locomotives is reducing the use of conventional diesel locomotives. However, in India, electricity production is also mainly dependent on coal-based thermal power plants, which also produces GHG emissions. IR has formed a separate entity called 'Indian Railways Organization for Alternate Fuels (IROAF)' to explore and assess newer alternative fuels for locomotive engines [24]. IROAF has explored fuels such as natural gas, di-methyl ether, methanol, etc., for locomotive traction. Several researchers have investigated methanol-diesel blends comprehensively [25-28]. Methanol usage in diesel locomotive has several challenges and needs comprehensive investigations.

Methanol miscibility with diesel is rather limited, restricting methanol usage to only ~10% (v/v) in the form of methanol-diesel blends [7]. Methanol-diesel blends with higher methanol fraction exhibit phase separation issues. Methanol enriched bottom phases may stall the engine unexpectedly [29]. Additives such as dodecanol, a mixture of Oleic acid, and Iso-butanol/ n-butanol have been explored to improve the miscibility of methanol-diesel blends [30-33]; however, use of additives affects overall physico-chemical properties of test fuel adversely. Their usage reduces particulate emissions; however, it depends on additives' molecular configuration [34].

Use of methanol in large-bore diesel engines always poses a challenge. There are couple of potential techniques for inducting methanol in large-bore locomotive engines such as (i) Port fuel injection (PFI), where methanol can be injected in the port, with diesel pilot injection as an ignition source, and (ii) High-pressure direct injection (HPDI), where methanol and pilot diesel both are injected directly into the engine cylinder. These techniques significantly facilitate methanol in diesel engines and are already tested by several researchers extensively in the test-cell [35-45]. They can reduce tailpipe emissions up to a great extent with comparable/ higher engine power output. HPDI method can be used in two ways, either by incorporating two separate injectors on the already crowded cylinder head, leading to cylinder head design complications, or by incorporating them in a single co-axial injector. Former approach warrants an electronically driven precise control system for controlling two injection events of two different fuels through two sets of injector nozzles. In the co-axial injection system, two injection events of two different fuels are controlled by a single injector body, which is an economical approach compared to the former one. Therefore, this study aims to assess HPDI technique using a co-axial injector through a simulation approach. In the direct injection engine, fuel-air mixing plays a vital role in combustion and subsequently affects engine performance and emissions. In-cylinder flow structures of a diesel engine are complex and vary significantly with different engine designs and sizes. In-cylinder phenomena such as charge-density distribution, temperature variations, spatial pressure variations are important characteristics that directly affect engine performance. In-cylinder flow characteristics also influence heat transfer, thereby entire in-cylinder flow structures. They can be characterized either experimentally or computationally. Experimental flow characterization can be achieved using an optical engine along with optical diagnostics tools. Besides, computational fluid dynamics (CFD) has also become an integral part of the engine development process due to its capability to predict and interpret in-cylinder flow-fields.

CFD uses numerical code to perform repetitive parameter studies with imposed boundary conditions. Multi-dimensional models reduce the need for physical experiments, leading to an enormous reduction in product development time and cost [37]. Although several commercial CFD packages are currently available in the market, CONVERGE CFD is the most widely used software for 3-D simulations of IC engines. It enables autonomous meshing, which encompasses an entire set of robust and innovative grid-related capabilities. CONVERGE automatically creates a mesh with optimum run-time, dynamically adapts the mesh throughout the simulation domain and invokes adaptive mesh refinement (AMR) to maximize both the accuracy and the computational efficiency. In this investigation, we have attempted to model a locomotive engine in Converge CFD to understand spatial and temporal variations of different parameters such as in-cylinder pressure variations, temperature variations, fuel-air mixing processes, etc. Detailed comparative analysis has been done, where 90% diesel replacement on an energy basis was done by methanol, which was ignited by pilot diesel that provided 10% of the energy.

Methodology

In the present study, prediction of locomotive engine's cylinder behaviour with diesel fueling and methanol fueling was targeted through simulation approach. In this study, direct injection of methanol using HPDI technique was selected for modeling and analysis. This was based on the experimental study done at Engine Research Laboratory (ERL) IIT Kanpur and RDSO Lucknow on lower methanol-diesel blends. Experiments concluded that methanol and diesel have poor miscibility, and it was not possible to run the engine with methanol diesel blend, where more than 10% (V/V) diesel was displaced by methanol. In the port injection method, methanol was injected during the intake stroke to make a homogeneous mixture. However, at low speed, the fuel-air mixture becomes very lean for the locomotive engine. It is difficult to ignite the mixture because it goes beyond the ignitibility limit. This method may result in high-cold start emission as well. In the direct injection method, methanol is injected towards the end of the compression stroke; thereby, a locally rich mixture is formed, which is easy to ignite. Port fuel injection (PFI) technique of methanol in the intake stroke might be a viable technique for smaller engines; however, for locomotive engine it is not suitable, and therefore, this strategy is discarded. Four stage plans were executed, as shown in Figure 1. Data collection exercise was performed at RDSO Lucknow for the diesel-fueled ALCO-251 locomotive engine in the first stage. Locomotive engine works at eight different notches, which represent different engine speeds: (i) 350 rpm (1st Notch) (ii) 450 rpm (2nd Notch) (iii) 550 rpm (3rd Notch) (iv) 650 rpm (4th

FIGURE 1 Methodology flow chart of the present study.

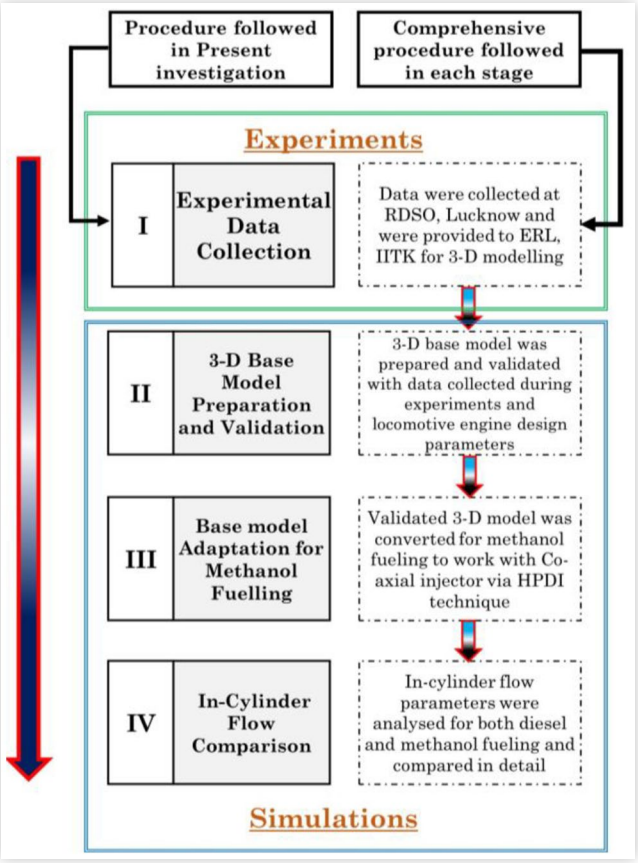

Notch) (v) 750 rpm (5th Notch) (vi) 850 rpm (6th Notch) (vii) 950 rpm (7th Notch) and (viii) 1050 rpm (8th Notch). Notching up the engine leads to an increase in engine speed and power almost linearly. In the second stage, CAD model of locomotive was prepared, and case setup was done using Converge Studio. This virtual model was validated using the experimental in-cylinder pressure traces logged during the data collection for the 8th notch. In the third stage, validated 3-D model was converted for methanol fueling such that it adopts a co-axial injector for implementation of HPDI technique. A comparative analysis of the in-cylinder phenomenon of diesel fueling and methanol fueling was performed in the last stage. For analysis, Tecplot from the Converge was used. The flow chart of the methodology followed in this study is shown in Figure 1.

Stage 1: Test Data Collection for Diesel Fueled Locomotive Engine

The selected ALCO-251 locomotive engine was sixteen cylinders, V-configuration, turbo-charged, after-cooled, four-stroke CI engine. It has deep-bowl pistons, and the cylinder head was flat. Engine had an overhead valve setup, and camshafts were below the cylinder head. Technical specifications of the test engine are listed in Table 1.

For loading the engine, a hydraulic dynamometer was coupled to it. For the measurement of various parameters such as pressure, temperature, engine speed, torque, flow rate, etc., suitable sensors were employed. A schematic experimental setup is given in Figure 2.

TABLE 1 Specifications of ALCO-251 locomotive test engine.

Parameters	Specifications
Engine Make/ Model	DLW/ ALCO 251-B engine
Engine Type	4-Stroke
No. of Cylinders	16
Cylinder Configuration	V
Compression Ratio	11.75
Bore × Stroke (m × m)	0.2286 × 0.2667
Firing Order	1R 1L, 4R 4L, 7R 7L, 6R 6L, 8R 8L, 5R 5L, 2R 2L, 3R 3L
Turbocharger	One
Aftercooler	Single, water-cooled
Max. Engine speed	1050 rpm
Fuel Injection Equipment	Mechanical, PLN Injection
Nozzle Opening Pressure	250 bar
Max. Fuel Injection Pressure	1200 bar
Rated Power	2312 kW @ 1050 rpm
IVO / IVC	50 CAD bTDC / 12 CAD aBDC
EVO/ EVC	40 CAD bBDC / 20 CAD aTDC

The locomotive engine was connected to a hydraulic dynamometer, which controlled its load and speed. The maximum power and torque rating of this dynamometer were 4400 kW and 47745 Nm, respectively. It was designed to operate at a maximum speed of 2500 rpm, which could be controlled by a dynamometer controller (AVL, EMCON 300). Control of loading conditions was achieved by varying the quantity of water flowing through the dynamometer. The dynamometer consists of a closed-loop water circuit and has a heat exchanger to control the flowing water temperature. This makes them suitable for steady-state testing of the locomotive engine for a long duration. Present investigations were carried out at pre-defined steady-state conditions at different locomotive engine notches. Essential data were collected to carry out engine performance, combustion, and emissions characterizations.

Engine load control can be achieved with the help of a hydraulic dynamometer, and the fuel mass injection control was accomplished with the use of a fuel actuator. Air from the compressor passed through an intercooler, followed by its

FIGURE 2 Schematic of the locomotive engine test cell.

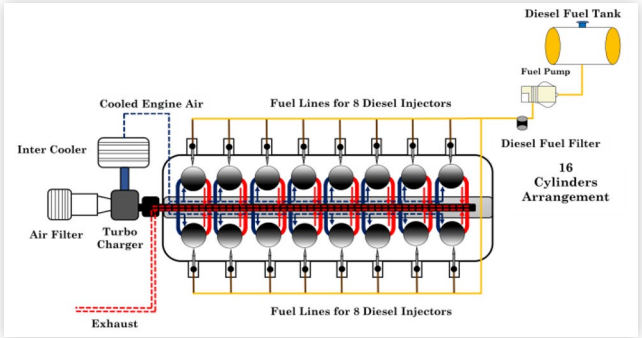

supplement to the individual engine cylinders through individual air-inlet manifolds. Exhaust from the engine passed through the turbine outlet of the turbocharger, which was eventually discharged into the atmosphere via the exhaust outlet duct.

Stage 2: 3-D Base Model Preparation

Before proceeding for case-setup, CONVERGE required a CAD model in Stereolithography (STL) format. Initially, CAD model of the piston was developed using Unigraphics (UG-NX) modeling software. Front and top views of the prepared CAD model of the piston are given in Figure 3. For the sake of understanding, the spatial and temporal variations model were set to run at top-notch (1050 rpm). CONVERGE comprises of two utility software along with a solver (See Appendix A and B). Case-setup and initial geometrical interpretations were made in converge studio, and post-processing of 3-D output was accomplished in Tecplot for converge. CAD model was imported into Converge Studio for geometrical interpretation, such as setting-up boundary conditions and finding intersecting triangles, etc.

FIGURE 3 Different views of CAD model of locomotive piston.

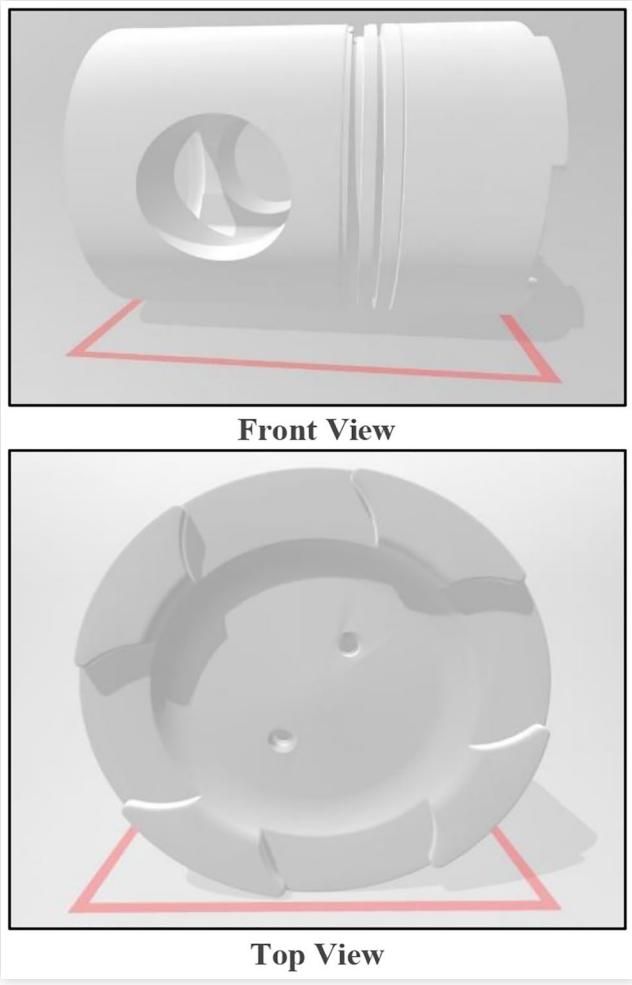

For making a computational domain, piston bowl profile was extracted first from the surface.dat file. Depending on the accuracy and requirement of the crevice, profile is added. Here, if the nozzles are placed on an equal angle, then sector geometry simulation is preferred. Simulation of sector geometry offers advantage in terms of computational time.

Setup of Boundary Conditions: The computational domain mainly comprises of three-boundary regions: Head, Liner, and Piston Surfaces, as shown in Figure 4.

In Converge Studio, all three boundaries are set as 'wall-type'. However, only piston is set to translating wall motion type, and head and liner are set to stationary with no surface movement. Initial temperature at different boundary conditions is taken, as shown in Table 2.

'Law of the wall' is recommended for high Reynolds number flow. IC engine combustion chambers have a highly turbulent flow, which has very high Reynolds number. At the wall boundary, temperature and velocity are calculated using the 'law of the wall'. Rough constant in the law of the wall parameter is set to 0.5. Newman boundary condition is set for turbulent kinetic energy (TKE) boundary condition. In the law of the wall, CONVERGE uses a logarithmic curve fit method for calculation of fluid velocity at the wall boundary. As stated previously, 3-D CFD analysis is carried out using commercial software, CONVERGE CFD. In this software, run time mesh is generated using the cut-cell Cartesian method. Here the base grid size is kept at 4 mm. The spatial mesh refinement at the injector location is performed using a fixed embedding technique for a specified period. Further, AMR is used to capture the velocity and temperature gradients, once it crosses the threshold. IC engine involves a complex mixing process in the combustion chamber. Governing differential equations for the dynamics of fluid flow is conservation of mass, momentum, and energy equations. Additional governing equation are required, which

FIGURE 4 Computational domain showing different boundary-regions.

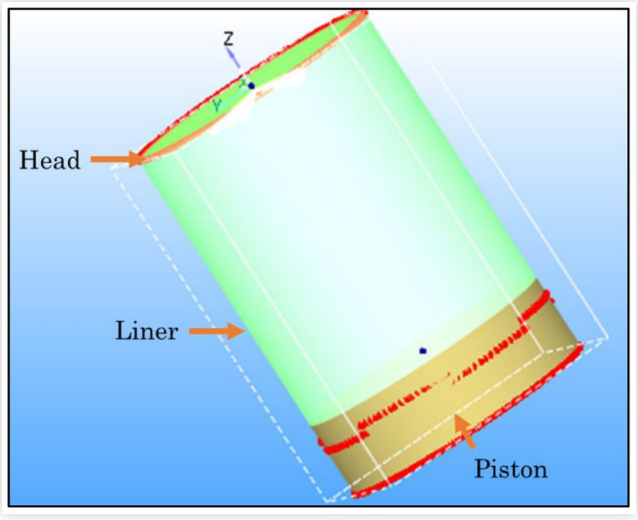

TABLE 2 Temperature boundary conditions.

Boundary	Temperature (K)
Piston	550
Liner	460
Head	500

describe the turbulence and transport of passive scalar, and species. The in-cylinder fluid is considered as compressible fluid. Equations for mass, momentum, and energy transport are as follows [46]:

$$\frac{\partial \rho}{\partial t} + \frac{\partial \rho u_i}{\partial x_i} = S \tag{I}$$

$$\frac{\partial \rho u_i}{\partial t} + \frac{\partial \rho u_i u_j}{\partial x_j} = -\frac{\partial P}{\partial x_i} + \frac{\partial \sigma_{ij}}{\partial x_j} + S_i \tag{II}$$

Where the viscous stress tensor (σ_{ij}) is given by:

$$\sigma_{ij} = \mu\left(\frac{\partial u_i}{\partial x_j} + \frac{\partial u_j}{\partial x_i}\right) + \left(\mu' - \frac{2}{3}\mu\right)\left(\frac{\partial u_k}{\partial x_k}\delta_{ij}\right) \tag{III}$$

$$\frac{\partial \rho e}{\partial t} + \frac{\partial u_j \rho e}{\partial x_i} = -P\frac{\partial u_j}{\partial x_j} + \sigma_{ij}\frac{\partial u_i}{\partial x_j} + \frac{\partial}{\partial x_j}\left(K\frac{\partial T}{\partial x_j}\right) + \frac{\partial}{\partial x_j}\left(\rho D\sum_m h_m \frac{\partial Y_m}{\partial x_j}\right) + S \tag{IV}$$

Here, u is the velocity; ρ is the density; S is the source term; P is the pressure; σ_{ij} is the viscous stress tensor; Y_m is the mass fraction of species m; D is the mass diffusion coefficient; e is the specific internal energy; K is the conductivity; h_m is the species-specific enthalpy; and T is the temperature. μ' is the viscosity, and δ_{ij} is the Kronecker delta. It is essential to solve the mass and momentum equations simultaneously for calculating pressure gradient in the momentum equation.

Turbulence Modeling: Turbulence is modelled using RNG k-ε model. These models are two-equation RANS models, in which the flow variables (velocity, temperature, pressure) are decomposed into an ensemble mean and a fluctuating term. It is a commonly used model for IC engine applications. For accommodating the effect of small-scale gas motion, RNG (re-normalization group) model is developed, which renormalizes the N-S equations. In the k-ε model, a single turbulence length-scale was used for determination of eddy viscosity. Thus, calculated turbulent diffusion using k-ε model occurs only at specified turbulent scales. However, all scale of motion will contribute to turbulent diffusion. To account for turbulence diffusion from smaller scale motion, RNG model uses a mathematical technique to derive the turbulence model, which attempts to account for different scales of motion through changes to the production term. Turbulence parameters are given in Table 3.

Spray Modeling: Kelvin-Helmholtz (KH) and Rayleigh-Taylor (RT) models have been used to predict liquid atomization and spray droplet breakup. KH-RT analysis considers

TABLE 3 Turbulence parameters used in modeling of locomotive engine.

Turbulence Parameter	Value
Von Karman's constant	0.42
Law of the wall parameter	5.5
Wall heat transfer model	Angelberger
Cμ	0.0845
Reciprocal TKE Prandtl	1.39
Reciprocal E Prandtl	1.39

the stability of a cylindrical, viscous, liquid jet of radius (r_o) issuing from a circular orifice at a velocity U into a stagnant, incompressible, inviscid gas of density (ρ_g). For the liquid fuel having density ρ_l, viscosity μ_l, a cylindrical polar coordinate system was used which moved along with the jet. An arbitrary infinitesimal displacement was imposed on the initial steady motion. Arbitrary displacement was considered as an exponential form in the dispersion relation, which correlated the real part of the growth rate and the wave number. KH model was used to predict the initial breakup of the injected blobs/ intact liquid core. Rayleigh-Taylor (RT) model was then used in conjunction with KH model to predict secondary breakup of the droplets. RT model predicted instabilities on the surface of the drops, that grew until a characteristic breakup time when the drops finally broke-up. To incorporate the diesel droplets evaporation, Frossling evaporation model was selected with source specified species as an evaporation source. O'Rourke model was used to estimate the number of droplet collisions and their outcome in a relatively computationally efficient manner, which was made by the parcel concept. It is easy to correlate that for N drops, each having N-1 possible collision partners, the number of possible collision pairs is approximately (1/2) N^2. Without the parcel concept, this N^2-dependence would render the collision calculations computationally prohibitive for millions of droplets that may exist in a simulation. Different spray parameter that has been used during modeling are mentioned in Table 4.

Injector Specifications: A high-pressure fuel injector is located at the center of the cylinder axis. It consists of nine nozzle holes having a spray angle of 9 degrees (Figure 5). Detailed specifications of the base model fuel injector are given in Table 5.

TABLE 4 Spray parameter used for the base modeling.

Parameter	Value
Turbulent Dispersion	O'Rourke model
Evaporation Source	Source (C_7H_{16}) specified species
Collision Model	No Time Counter (NTC) Collision
Sprat breakup Model	KH-RT
Fraction of injected masa/parcel	0.05
Shed mass constant	1.0
KH-Model breakup time constant	7.0
RT- Model breakup time constant	1.0

FIGURE 5 Top view of the base model with nine nozzle hole injector.

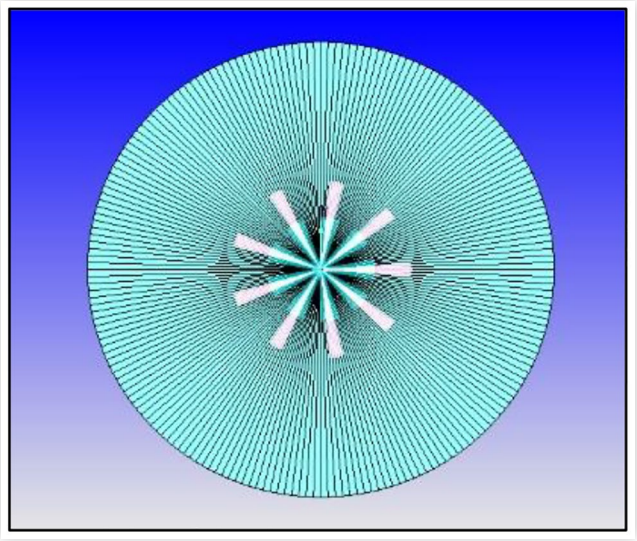

TABLE 5 Fuel injector specifications.

Parameter	Value
Fuel	Diesel
No. of nozzles	9
Diameter of nozzle (mm)	0.35
Circular Injection radius (mm)	0.259
Length of the nozzle (mm)	0.02
Spray cone angle (CAD)	9
Nozzle radial position (mm)	1
Nozzle axial position (mm)	5.28
Start of injection (SoI)	-17.86
Injection duration (CAD)	30
Total injected mass (kg)	0.000945
Total number of injected parcel (per nozzle)	712946

Stage 3: Base Model Conversion for Methanol Adaption Locomotive Engine

After validating the base-model with experimental data, existing model was converted such that it can be used for methanol fueling via HPDI technique. For M+D (methanol (90 %) with pilot diesel (10%) on energy basis) model, number of nozzles for pilot diesel injection were three, and methanol (main) injection was five, which destroyed symmetry. Hence, full sector geometry was simulated for diesel as well as M+D model for spatial comparison. However, injector specifications of co-axial injector were extracted from 1-D simulation study, and model was set to run with optimized dimensions for methanol and diesel. Injector specifications for M+D model are listed in Table 6. Top view of the M+D model with three nozzles for diesel injection and five nozzles of Methanol injection in a co-axial injector are given in Figure 6.

Combustion Modeling: In the present study, SAGE detailed chemistry solver was used. SAGE model was used to solve detailed chemical kinetics involved in the reactions and could predict both premixed and non-premixed combustion. Premixed combustion requires that the fuel and air be completely mixed before the combustion starts. Premixing is only executed at low temperatures, which do not allow the chain breaking mechanism to happen. However, in the present case, diesel engine is being simulated; hence premixing is not a major issue. In diesel engine, fuel is injected during compression stroke close to TDC, which is followed by four distinct phases of combustion, which include ignition delay, premixed combustion, mixing controlled combustion and late combustion. As mentioned earlier, SAGE detailed chemical kinetics solver was used in the present study, which can handle much of the chemistry taking place in the engine cylinder. However, SAGE detailed chemistry requires significantly longer run-time compared to other approaches. A chemical reaction mechanism is a set of elementary reactions that describe an overall chemical reaction. Combustion of different fuels can be modelled by changing the mechanism. Combustion modeling parameters are listed in Table 7.

For Methanol + Diesel model, a similar setting was used, except for fuel species. Fuel species were changed to Methanol (CH_3OH) and diesel, instead of diesel alone. Since, in Methanol + Diesel model, methanol was 90% by energy, which primarily dominated the combustion.

TABLE 6 Fuel Injector specifications for M+D model.

Parameter	Value
Fuel	Methanol (90% v/v) Diesel (10 % v/v)
No. of nozzles for Methanol injection	5
No. of nozzles for diesel injection	3
The diameter of nozzle for Methanol injection (mm)	0.544
The diameter of nozzle for diesel injection (mm)	0.486
Circular Injection radius for Methanol injection (mm)	0.175
Circular Injection radius for diesel injection (mm)	0.259
Length of the nozzle (mm)	0.02
Spray cone angle (CAD)	9
Nozzle radial position (mm)	1
Nozzle axial position (mm)	5.28
Start of Injection (SoI) for Methanol	-14.5
Start of Injection (SoI) for diesel	-16.4
Injection Duration (CAD) for Methanol injection	27
Injection Duration (CAD) for diesel injection	5
Total Injected mass of methanol (kg)	0.0017256
Total injected mass of diesel (kg)	0.0000945
Total number of injected parcels for methanol (per nozzle)	2300800
Total number of injected parcels for diesel (per nozzle)	208888

FIGURE 6 Top view of M+D model with 3 nozzles for pilot diesel and 5 nozzles for Methanol injection in a co-axial injector.

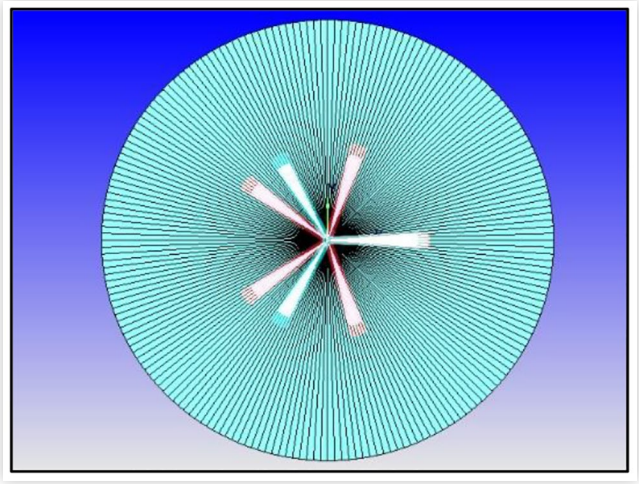

TABLE 7 Combustion modeling parameter for the base model.

Parameter	Value
Fuel species	C_7H_{16}
Temporal type	Sequential
Start Time	-19 CAD
End Time	133
Combustion Model	SAGE Detailed chemical kinetics solver
Re-solve temperature	2.0 K
Reaction multiplier	1.0
Adaptive zoning	Yes

Stage 4: In-Cylinder Flow Comparison

In this stage, in-cylinder flow parameters were analyzed using Tecplot software (See Appendix B). First, parameters were extracted for base model, and pressure data comparison was performed using line plots available in Converge Studio. 3-D output enables for observing the spatial and temporal variations for both models. The surface output (3D) from solver was first converted into Tecplot readable file in Converge Studio. In the Tecplot the result obtained from solver was imported, and contour plot of in-cylinder velocity, temperature, and density variation for both the base and M+D model were observed and compared. For analysis of flow structure before and after injection velocity magnitude plots were extracted.

Results and Discussion

Since 1-D model does not give information about the in-cylinder phenomenon, 3-D model of ALCO-251 was prepared for this analysis. Prepared 3-D model needs to be validated with experimental test data. For validation, experimental data was collected at the top-notch (8^{th} notch). All other notches are expected to exhibit similar characteristics.

P-θ Diagram Validation

For validation of 3-D model, P-θ history was selected. Validation of P-θ was done in a stepwise manner. First, the in-cylinder trapped mass was validated. For validating the trapped mass, initial temperature and pressure were tuned in such a way that they matched with the experimental data. From Figure 7, it can be observed that predicted pressure was in good agreement with the measured pressure. However, the deviation started near the TDC, and the maximum deviation was ~5.2% at 9° aTDC. Slight disagreement was mainly because of various assumptions made, while modeling. 3-D output was the surface output associated with different parameter. 3-D results helped us in analyzing spatial variations of a given parameter in the engine cylinder.

Once the base model was validated with acceptable accuracy, different results were exported for further analysis. Thereafter, M+D model was built in the Converge studio in a similar fashion, and optimized injector dimensions from the GT power were invoked into this model. Two different injector rate shapes were employed for incorporating the main injection of methanol and pilot diesel injection.

Comparison of Different Simulation Results for Base Model and M+D Model

After ensuring the validation of the base model with experimental results, the methanol was modeled to displace 90% methanol on an energy basis. For the in-cylinder phenomena comparison, species mass concentration in the different temperature zone was compared for base and M+D model.

FIGURE 7 Validation of In-cylinder pressure Vs crank angle diagram at top-notch (1050 rpm) for ALCO-251 locomotive engine.

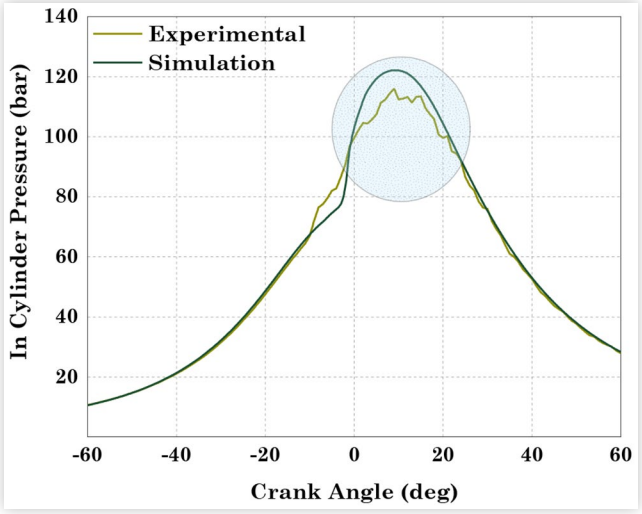

Thereafter, in-cylinder velocity, temperature, and density variation were observed for both the models, which have been discussed below.

In-Cylinder Species Mass Fraction in Different Temperature Zones In-cylinder species mass fraction changes with the temperature developed during combustion inside cylinder. Chemical reactions are the source term in the energy equation, wherein temperature changes from one place to another within the cylinder, depending on energy being transferred from one location to the other. In this study for simulating chemical kinetics of mineral diesel, n-heptane reaction mechanism was used. N-heptane was selected as a surrogate fuel for simulations because its chemical properties are similar to diesel, especially the cetane number [47]. Since diesel is in liquid state at normal operating condition, DIESEL-2 mechanism file was used for simulating the chemical kinetics of mineral diesel. This mechanism consists of 42 species and 168 elementary reactions.

Figure 8 shows the species mass fraction available at different temperature ranges for base model and M+D model. The maximum localized in-cylinder temperature in base-model reached up to ~2838 K, and in M+D model, it reached up to ~2673K. One can observe from Figure 8 that in the base model for diesel, the mass fraction at >2500 K temperature range was ~8%, which decreased to 4.3 and 2.1% respectively for temperatures >2600 K and >2700 K. Species mass fraction at > 2800 K for diesel was negligible and minimal fluctuations were observed in 5-10° CA aTDC. On the other hand, for M+D model of ALCO-251 locomotive engine, species mass fraction for temperature >2500 K was ~0.65%, which was very low compared to ALCO-251 modeled with only diesel (base model). This difference was even higher in the higher temperature zone. The in-cylinder species mass fraction for the temperatures >2700 K and >2800 K were negligible. This was in contrast to some species mass being present in base model for diesel. The difference was mainly attributed to methanol's lower latent heat of vaporization (LHV) compared to diesel. However, localized temperature variations may be different, as explained in the next section.

FIGURE 8 Species mass fraction in different temperature zones (> 2500 K) at different crank angles for the base and M+D models.

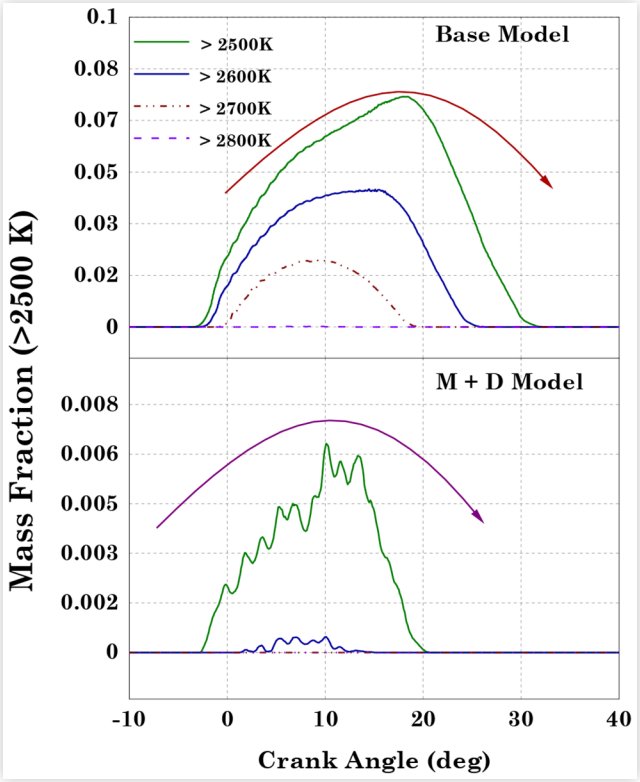

Species Concentration Variations with Crank Angle Figure 9 shows the species (O_2, CO_2, and CO) mass concentration variations for diesel and M+D model. It can be observed from figure 9 that the species O_2 mass concentration was almost the same up to -8 CAD for both diesel and Methanol models. However, beyond that, O_2 mass concentration was significantly higher for the locomotive engine operated with Methanol in HPDI (M+D model) compared to the diesel-fueled locomotive (base model). This was mainly because of methanol being an oxygenated fuel, having ~50% w/w oxygen in its molecular composition. CO and CO_2 species formations were relatively lower for the M+D model compared to the base model. However, the results presented here are only for the top-notch (1050 rpm) of the locomotive engine, and these trends may vary at lower notches.

In-Cylinder Flow Visualization

The in-cylinder flow of an internal combustion engine during the intake and compression strokes is one of the most important factors, that affects the combustion quality. The airflow structures in the intake stroke are primarily influenced by the intake port design, valve design, valve lift, timing, etc. Swirl and tumble motions are used to aid the air-fuel mixing and to enhance the combustion process. In this study, methanol is injected using high pressure direct injection; hence fuel-air mixing will also be a dominating factor to enhance the

FIGURE 9 CO, CO_2 and O_2 species mass concentration variations at different CAD for base model and M+D model.

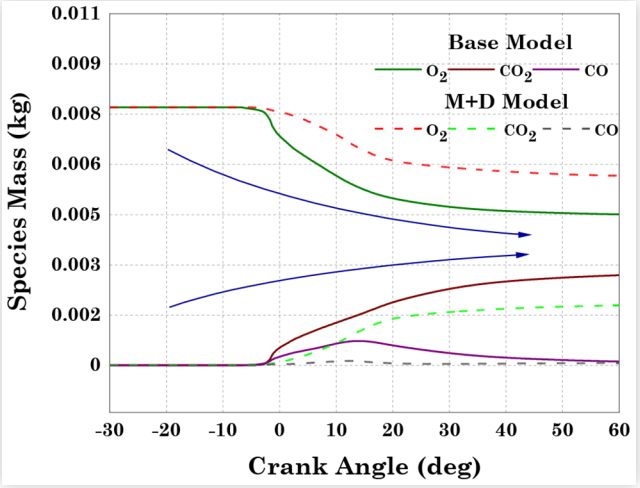

combustion efficiency. In this study, design of intake port and valve lift optimization is not being considered. The main objective is to test the viability of Methanol injection and its technical feasibility in existing ALCO-251 locomotive engines for co-axial injector using HPDI technique. Hence, the injection timing and injector dimensions were optimized for Methanol induction in the ALCO-251 locomotive engine. Therefore, flow characteristics were modelled in the compression stroke at 50, 40, 30 and 20 CAD bTDC.

Figure 10 shows the velocity distribution piston boundary and flow structure in compuataional domain. A vertical slice (YZ plane) were extracted which respresent the flow velocity vector. Since the fuel injection for both the base model and the M+D model starts after 20 CAD bTDC hence interpretations from Figure 10 will be applicable to both the models under investigation. From the figure 10, it can be observed that at -50 CAD, the maximum velocity reached up to 10 m/s at the cylinder head boundary. However, at the same time, the maximum velocity at the piston surface reached up to ~15 m/s. This result also matched with one similar study conducted by Perini et al. [48] on a smaller diesel engine. This difference is justified since in the compression stroke, kinetic energy of the charged particles at the piston boundary was higher when the piston moved upwards. In figure 10 (a) and (b), one can notice that the velocity was minimum at the centre at piston boundaries. As the piston approached TDC, the velocity variations were negligible at the piston boundary. Figure 11 shows the flow structure after the injection of fuel. The first column representing the flow structure for the base model at three different YZ plane at x=-60, 0, 60 mm, and the second column represents the same for the M+D model. In Figure 11(a) the diesel parcel distribution was presented, and in Figure 11(b), methanol with pilot diesel parcels was shown within the computational domain. The flow structure for base and M+D models was different at given planes. This difference was mainly because of the different injector configurations used for the M+D model compare to the base model.

FIGURE 10 Flow structures in the compression stroke from -50 to -20 CAD before injection (Column 1: contour plot the cylinder head boundary (vertical slice (YZ plane) at x=0 mm; and Column 2: contour plot at the piston boundary).

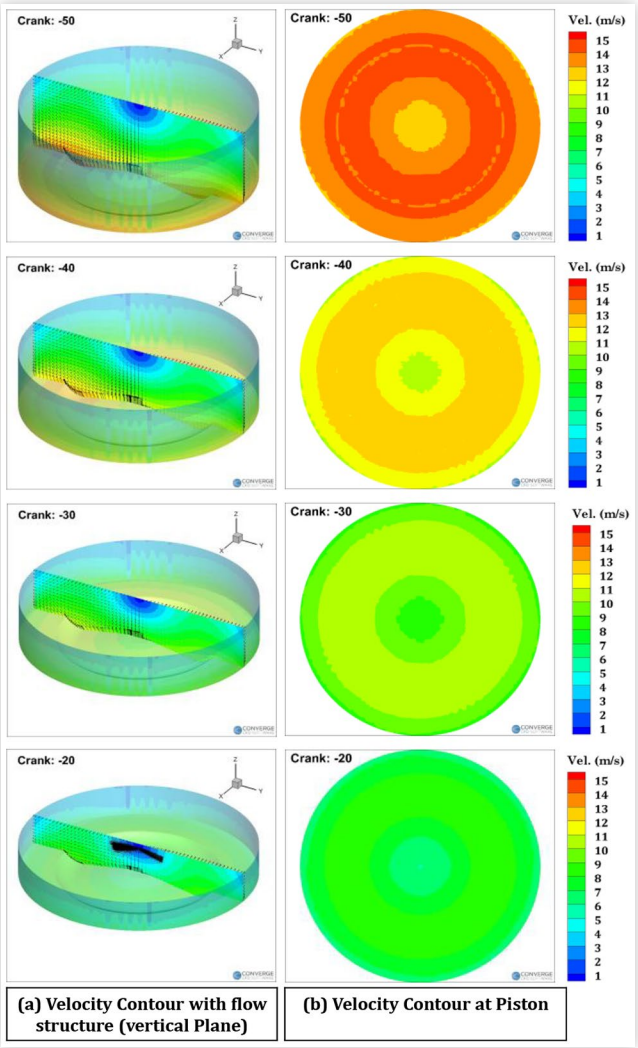

In-cylinder Temperature Variations Experimental measurement and analysis of in-cylinder temperature variations is not an easy task because of several constraints such as sensitivity of sensors and material compatibility. But simulations can be used for qualitative assessment of in-cylinder temperature variations. Figure 12 shows the in-cylinder

FIGURE 11 Flow structures in the compression stroke from -16 to -4 CAD after injection (Column 1: Base Model Column 2: M+D Model; three different vertical plane (YZ) at x=-60, 0, 60 mm).

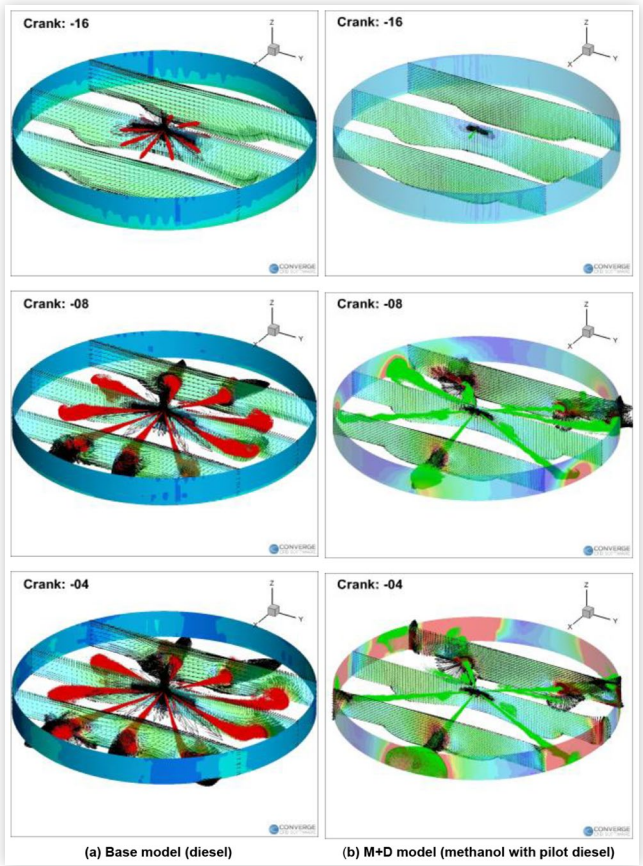

temperature variations for locomotive engine, ALCO-251 operated on diesel as well as methanol with pilot diesel via 3-D simulations in Converge. Spray distribution is also accommodated with temperature contours for both the models. Fuel spray parcel was shown in different colors. In base model, diesel spray was shown with red colour, and in M+D model, both methanol and pilot diesel was shown with green colour. From the temperature contour plot, it can be observed that the ignition starts in the region where diesel particles were present in higher concentration and out of three regions in the direction of diesel spray only two of them are ignited. One spray plume of diesel fuel gets coincide in the direction of methanol, where some cooling effects were present due to cooling nature of methanol.

At -16 CAD, base model shows nine sprays of diesel and M+D model shows only three sprays of pilot diesel. As piston approaches TDC, the pilot diesel disappears, which can be seen at -08 CAD and TDC in figure 12, and five sprays of methanol are visible in M+D model. Flame front propagation was observed for both models. In the locomotive engine fueled with diesel (base model), flames propagate in the direction of spray near the TDC and then propagates back into the combustion chamber. However, in methanol with pilot diesel model (M+D), flame propagation starts at the peripheral side, where rich air-pilot diesel mixture was present, and then flames propagate into the remaining engine cylinder. Methanol with pilot diesel exhibits dominantly homogeneous combustion, and only diesel exhibits dominantly heterogeneous combustion. The maximum localized in-cylinder temperature for diesel operated locomotive engine was ~2838K at ~8 CAD aTDC, and for methanol with pilot diesel, it was ~2673 K at ~5.5 CAD aTDC. This difference in the peak temperature values was mainly because of relatively lower heating value of methanol compared to diesel. Another possible reason could be more homogeneous mixture in M+D model because base-model mostly undergoes relatively more heterogeneous combustion. One can observe that at -16 CAD, the temperature distribution in each model is rather similar because this is the start of fuel injection for both models. However, after the injection of fuel, temperature contours are different in base-model and M+D model. Variations in temperature pattern is expected because the base model uses a nine-hole injector, whereas M+D model has eight-hole injector, three for pilot diesel injection and five for methanol injection. From the contour plots, it can be seen that during the compression stroke, the maximum temperature in the cylinder is ~600 K, which was sufficient to ignite the fuel-air mixture in both models. For the base model at TDC, one can observe that temperature reached up to ~900 K and followed a similar pattern along the spray direction, as observed from the iso-surfaces.

FIGURE 12 Flame front temperatures in the spray plume for base model as well as M+D model at different locations (slice view at Z=-14.7 mm).

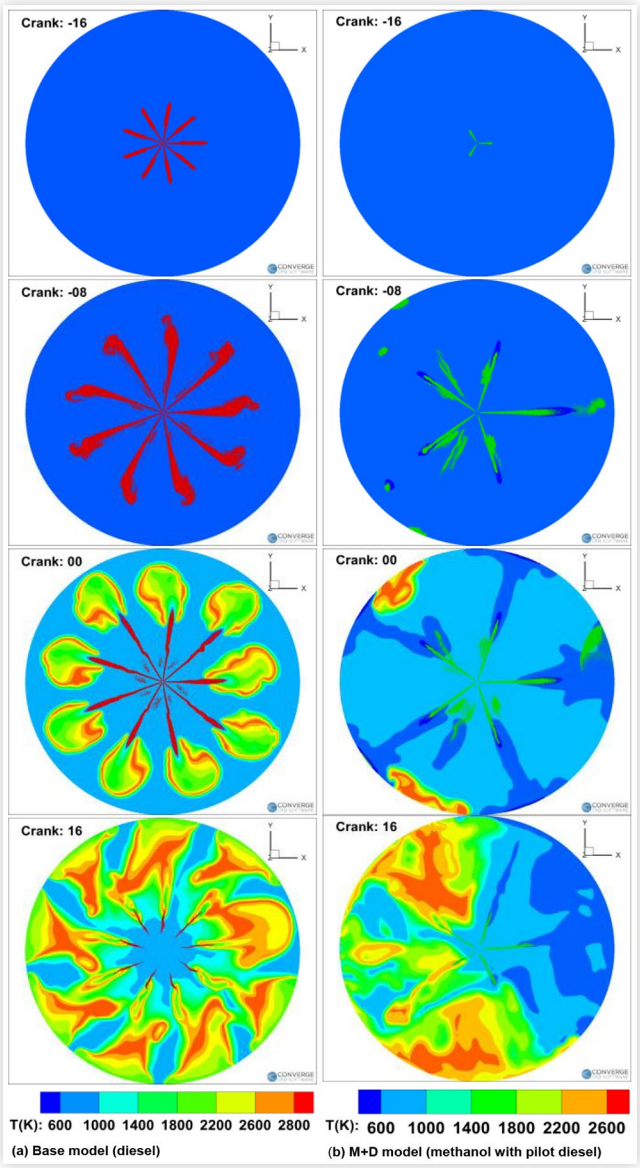

In-cylinder Density Variations

Charge density in diesel is an important parameter and is influenced by intake pressure, temperature, compression ratio, etc. Charge density strongly affects the initiation of combustion and combustion quality of the engine. Spray development is also affected by the charge density, and it resists spray penetration. Local charge density varies a lot until fuel injection, and consequent combustion gets completed. During fuel injection, local density in the vicinity of spray injection may be significantly higher, and after some time (attributed to physical and chemical delay), the fuel mixes with the air, and local density becomes uniform. Figure 13 shows the density variations in the ALCO-251 locomotive engine fueled with diesel (base-model) and methanol with pilot diesel (M+D model). Two different legend patterns are selected to clearly differentiate both the models. The maximum mean charge density for the base model reaches up to ~33 kg/m^{3,} and for the M+D model, it reaches up to ~27 kg/m^3. Density in case of M+D model is relatively lower, primarily due to two reasons. The first reason is that methanol (792 kg/m^3) has a lower density compared to diesel (830 kg/m^3), and the second reason is that in M+D model, charge exhibits greater mixture

FIGURE 13 In cylinder charge density variation for base model and M+D model.

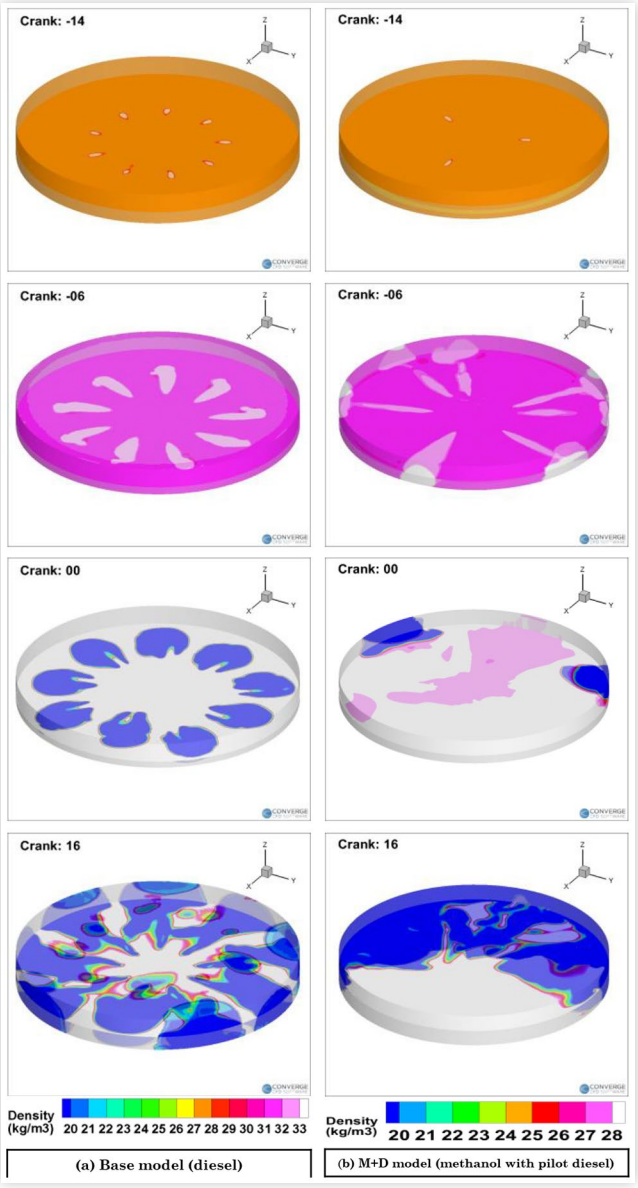

homogeneity compared to the base-model. At TDC, greater mixture homogeneity of M+D model can also be observed in the figure quite clearly. In both models, as the piston approaches the TDC, charge density increases, which is on expected line since the volume reduces due to compression and then the fuel is injected. At TDC, another observation is nine symmetric iso-surfaces, showing fuel concentration zones having much higher density compared to other locations in the combustion chamber in case of base-model. Both the models show different patterns for charge density distribution due to differences in number of injection nozzles and test fuels. From this density distribution contour plots, a conclusion can be drawn that methanol can be a good fuel candidate for ALCO-251 locomotive engines.

Conclusions

In this study, a 3-D model was built using CONVERGE software and validated using experimental data provided from RDSO for diesel fueling. The validated model was tuned to adapt methanol in the locomotive engine. A comparative study was done for the base model and M+D model. Species variations in different temperature zones was shown for the locomotive operated with methanol and pilot diesel vis-a-vis locomotive engine operated with only diesel. Major results have been shown following.

- It was concluded that species mass fraction at >2800 K for diesel was negligible.
- O_2 mass concentration was significantly higher, whereas CO and CO_2 species formations were relatively lower for M+D model compared to the base model.
- From the temperature contour plot, it was observed that when locomotive was fueled with methanol, the spray was more homogenous.
- Methanol sprays ended up striking the cylinder walls, and then droplets rebound and mixed with air. The maximum in-cylinder temperature for the diesel-fueled locomotive was ~2838K, while for HPDI of Methanol with pilot diesel, it was ~2673 K.
- A difference of ~150°C temperature was observed in the M+D model compared to the base model, which may be because the locomotive fueled with methanol makes dominantly homogenous mixture compared to diesel-fueled locomotive. Another possible reason could be that fuel injection pattern was different in both models. Base-model used a 9-hole injector, whereas M+D model used an 8-hole injector, which had three nozzle holes for pilot diesel injection, and five nozzle holes for Methanol injection.
- At TDC, greater charge homogeneity in the M+D model was observed. In both models, as the piston approached TDC, charge density increased because the cylinder volume reduced due to compression, and then the fuel was injected. Both models showed different charge density distributions due to differences in injection strategies and test fuels.

Overall, from the in-cylinder species variations and variations in parameters such as temperature and density, it can be concluded that methanol can be a substitute to diesel for locomotive engines.

Future Work and Limitation

- The assessment of methanol fueling presented in the manuscript was purely based on 3-D simulation.

- In-Cylinder flow behavior could be seen through Particle Image Velocimetry for getting more confidence on the results.
- Proposed co-axial injector as per configuration needs to be manufactured for the experimental validation of performance, emissions, and combustion characteristics.
- Physico-chemical properties of fuel were directly taken from 3-D converge software. In reality, it could be slightly varied.

References

1. Agarwal, A.K., "Biofuels (Alcohols and Biodiesel) Applications as Fuels for Internal Combustion Engines," *Progress in energy and combustion science*, 1;33(3):233-71, 2007, doi: 10.1016/j.pecs.2006.08.003.
2. Rakopoulos, C.D.., Antonopoulos, K.A.., Rakopoulos, D.C.., "Experimental Heat Release Analysis and Emissions of a HSDI Diesel Engine Fueled with Ethanol-Diesel Fuel Blends," *Energy*, 1;32(10):1791-808, 2007, doi: 10.1016/j.energy.2007.03.005.
3. Xingcai, L., Zhen, H., Wugao, Z., Degang, L.,. "The Influence of Ethanol Additives on the Performance and Combustion Characteristics of Diesel Engines," *Combustion Science and Technology*, 1;176(8):1309-29, 2004, doi: 10.1080/00102200490457510.
4. Shahabuddin, M., Liaquat, A.M.., Masjuki, H.H.., Kalam, M.A.., Mofijur, M., "Ignition Delay, Combustion and Emission Characteristics of Diesel Engine Fueled with Biodiesel," *Renewable and Sustainable Energy Reviews* 1;21:623-32, 2013, doi: 10.1016/j.rser.2013.01.019.
5. Arcoumanis, C., Bae, C., Crookes, R., Kinoshita, E., "The Potential of Di-methyl Ether (DME) as an Alternative Fuel for Compression-Ignition Engines: A Review," *Fuel* 1;87(7):1014-30, 2008, doi: 10.1016/j.fuel.2007.06.007.
6. Yao, C., Cheung, C.S.., Cheng, C., Wang, Y., "Reduction of Smoke and NO x from Diesel Engines using a Diesel/Methanol Compound Combustion System," *Energy & Fuels* 21;21(2):686-91, 2007, doi: 10.1021/ef0602731.
7. Valera, H., Agarwal, A.K.., "Methanol as an Alternative Fuel for Diesel Engines," In *Methanol and the Alternate Fuel Economy* (pp. 9-33). Springer, Singapore, 2019, doi: 10.1007/978-981-13-3287-6_2.
8. Zhen, X., Wang, Y., "An Overview of Methanol as an Internal Combustion Engine Fuel," *Renewable and Sustainable Energy Reviews* 1;52:477-93, 2015, doi: 10.1016/j.rser.2015.07.083.
9. Methanol Economy-India "Methanol Economy," https://niti.gov.in/methanol-economy, Accessed Nov. 2020.
10. Li, Z., Gao, D., Chang, L., Liu, P., Pistikopoulos, E.N.., "Coal-Derived Methanol for Hydrogen Vehicles in China: Energy, Environment, and Economic Analysis for Distributed Reforming," *Chemical Engineering Research and Design* 1;88(1):73-80, 2010, doi: 10.1016/j.cherd.2009.07.003.
11. Yang, C.J.., Jackson, R.B.., "China's Growing Methanol Economy and Its Implications for Energy and the Environment," *Energy Policy* 1;41:878-84, 2012, doi: 10.1016/j.enpol.2011.11.037.
12. Valera, H., and Agarwal, A.K., "Future Automotive Powertrains for India: Methanol Versus Electric," *Alternative Fuels and Their Utilization Strategies in Internal Combustion Engines* 10:89, 2019, doi:10.1007/978-981-15-0418-1_7.
13. Mukherjee, A., Maity, A., Chatterjee, S., "Enabling a gasification and carbon capture economy in India: An integrated techno-economic analysis," Fuel, 1;263:116595, 2020, doi: 10.1016/j.fuel.2019.116595.
14. Gräbner, M., *Industrial Coal Gasification Technologies Covering Baseline and High-Ash Coal* (John Wiley & Sons, 2014), doi:10.1002/9783527336913.ch01.
15. Çelebi, Y., and Aydın, H., "An Overview on the Light Alcohol Fuels in Diesel Engines," *Fuel* 236:890-911, 2019, doi:10.1016/j.fuel.2018.08.138.
16. Zhu, L., Cheung, C.S., Zhang, W.G., and Huang, Z., "Emission's Characteristics of a Diesel Engine Operating on Biodiesel and Biodiesel Blended with Ethanol and Methanol," *Science of The Total Environment* 408(4):914-921, 2010, doi:10.1016/j.scitotenv.2009.10.078.
17. Liu, Y., Jiao, W., and Qi, G., "Preparation and Properties of Methanol-Diesel Oil Emulsified Fuel under High-Gravity Environment," *Renewable Energy* 36(5):1463-1468, 2011, doi:10.1016/j.renene.2010.11.007.
18. Zhang, Z.H., Cheung, C.S., Chan, T.L., and Yao, C.D., "Emission Reduction from Diesel Engine Using Fumigation Methanol and Diesel Oxidation Catalyst," *Science of The Total Environment* 407(15):4497-4505, 2009, doi:10.1016/j.scitotenv.2009.04.036.
19. Cheung, C.S., Zhu, L., and Huang, Z., "Regulated and Unregulated Emissions from a Diesel Engine Fueled with Biodiesel and Biodiesel Blended with Methanol Atmospheric Environment," 43(32):4865-4872, 2009, doi:10.1016/j.atmosenv.2009.07.021.
20. Cheng, C.H., Cheung, C.S., Chan, T.L., Lee, S.C. et al., "Comparison of Emissions of a Direct Injection Diesel Engine Operating on Biodiesel with Emulsified and Fumigated Methanol," *Fuel* 87(10-11):1870-1879, 2008, doi:10.1016/j.fuel.2008.01.002.
21. Valera, H., Singh, A.P., Agarwal, A.K., "Prospects of Methanol-Fuelled Carburetted Two Wheelers in Developing," *Advanced Combustion Techniques and Engine Technologies for the Automotive Sector*, p. 53, 2019, doi: 10.1007/978-981-15-0368-9_4.
22. "Global Diesel Engine Market Outlook 2020-2025," https://www.globenewswire.com/news-release/2020/10/06/2104126/0/en/Global-Diesel-Engine-Market-Outlook-2020-2025-Growth-in-Hybrid-Vehicles-Growth-in-the-Non-Automotive-Market.html, Accessed Nov. 2020.
23. "Share of diesel engine market across India in FY 2015, by type of end consumer," https://www.statista.com/statistics/744948/india-diesel-engine-market-share-by-end-consumer/, Accessed Nov. 2020.
24. "Indian Railway Organization for Alternative Fuels," https://iroaf.indianrailways.gov.in/, Accessed Nov. 2020.

25. Agarwal, A.K.., Shukla, P.C.., Patel, C.., Gupta, J.G.., Sharma, N.., Prasad, R.K.., Agarwal, R.A.., "Unregulated Emissions and Health Risk Potential from Biodiesel (Kb5, Kb20) and Methanol Blend (M5) Fueled Transportation Diesel Engines," *Renewable Energy* 1;98:283-91, 2016, doi: 10.1016/j.renene.2016.03.058.
26. Nagafi, G. and Yusaf, T.F., "Experimental Investigation of using Methanol-diesel Blended Fuels in Diesel Engine," in *Proceedings of the Fourth International Conference on Thermal Engineering: Theory and Applications* p. 1-5, Abu Dhabi, UAE, 2009.
27. Huang, Z., Lu, H., Jiang, D., Zeng, K., Liu, B., Zhang, J., Wang, X., "Combustion Behaviors of a Compression-Ignition Engine Fueled with Diesel/Methanol Blends under Various Fuel Delivery Advance Angles," *Bioresource technology.* 1;95(3):331-41, 2004, doi: 10.1016/j.biortech.2004.02.018.
28. Chao, M.R.., Lin, T.C.., Chao, H.R.., Chang, F.H.., Chen, C.B.., "Effects of Methanol-Containing Additive on Emission Characteristics from a Heavy-Duty Diesel Engine," *Science of the Total Environment* 12;279(1-3):167-79, 2001, doi: 10.1016/S0048-9697(01)00764-1.
29. Kumar, S., Cho, J.H.., Park, J., Moon, I., "Advances in Diesel-Alcohol Blends and their Effects on the Performance and Emissions of Diesel Engines," *Renewable and Sustainable Energy Reviews* 1;22:46-72, 2013, doi: 10.1016/j.rser.2013.01.017.
30. Murayama, T., Miyamoto, N., Yamada, T., Kawashima, J.I., and Itow, K., "A Method to Improve the Solubility and Combustion Characteristics of Alcohol—Diesel Fuel Blends," *SAE Transactions* 1:3485-3494, 1982, doi:10.4271/821113.
31. Huang, Z.H.., Lu, H.B.., Jiang, D.M.., Zeng, K.., Liu, B.., Zhang, J.Q.., Wang, X.B.., "Engine Performance and Emissions of a Compression Ignition Engine Operating on the Diesel-Methanol Blends," *Proceedings of the Institution of Mechanical Engineers, Part D: Journal of Automobile Engineering* 1;218(4):435-47, 2004, doi: 10.1243%2F095440704773599944.
32. Bayraktar, H.,. "An Experimental Study on the Performance Parameters of an Experimental Ci Engine Fueled With Diesel-Methanol-Dodecanol Blends," *Fuel* 1;87(2):158-64, 2008, doi: 10.1016/j.fuel.2007.04.021.
33. Valera, H. An experimental study on the physico-chemical properties, performance parameter in a CI engine fueled with methanol blended diesel (MBD) M. Tech Thesis, Department of Mechanical Engineering, Dr. B.R. Ambedkar National Institute of Technology (India), August 2017
34. Kitamura, T., Ito, T., Senda, J., Fujimoto, H., "Extraction of the Suppression Effects of Oxygenated Fuels on Soot Formation using a Detailed Chemical Kinetic Model," *JSAE review* 1;22(2):139-45, 2001, doi: 10.1016/S0389-4304(00)00108-9.
35. Pan, W., Yao, C., Han, G., Wei, H., Wang, Q., "The Impact of Intake Air Temperature on Performance and Exhaust Emissions of a Diesel Methanol Dual-Fuel Engine," *Fuel* 15;162:101-10, 2015, doi: 10.1016/j.fuel.2015.08.073.
36. Shamun, S., Haşimoğlu, C., Murcak, A., Andersson, Ö., Tunér, M., Tunestål, P., "Experimental Investigation of Methanol Compression Ignition in a High Compression Ratio Hd Engine using a Box-Behnken Design," *Fuel* 1;209:624-33, 2017, doi: 10.1016/j.fuel.2017.08.039.
37. Geng, P., Yao, C., Wei, L., Liu, J., Wang, Q., Pan, W., Wang, J., "Reduction of PM Emissions from a Heavy-Duty Diesel Engine with Diesel/Methanol Dual Fuel," *Fuel* 1;123:1-1, 2014, doi: 10.1016/j.fuel.2014.01.056.
38. Wei, H., Yao, C., Pan, W., Han, G., Dou, Z., Wu, T., Liu, M., Wang, B., Gao, J., Chen, C., Shi, J., "Experimental Investigations of the Effects of Pilot Injection on Combustion and Gaseous Emission Characteristics of Diesel/Methanol Dual-Fuel Engine," *Fuel* 15;188:427-41, 2017, doi: 10.1016/j.fuel.2016.10.056.
39. Li, G., Zhang, C., and Li, Y., "Effects of Diesel Injection Parameters on the Rapid Combustion and Emissions of an HD Common-Rail Diesel Engine Fueled with Diesel-Methanol Dual-Fuel," *Applied Thermal Engineering* 108:1214-1225, 2016, doi:10.1016/j.applthermaleng.2016.08.029.
40. Liu, J., Yao, A., Yao, C., "Effects of Diesel Injection Pressure on the Performance and Emissions of a HD Common-Rail Diesel Engine Fueled with Diesel/Methanol Dual Fuel," *Fuel* 15;140:192-200, 2015, doi: 10.1016/j.fuel.2014.09.109.
41. Wu, T., Yao, A., Yao, C., Pan, W., Wei, H., Chen, C., Gao, J., "Effect of Diesel Late-Injection on Combustion and Emissions Characteristics of Diesel/Methanol Dual Fuel Engine," *Fuel* 1;233:317-27, 2018, doi: 10.1016/j.fuel.2018.06.063.
42. Singh, A.P., Sharma, N., Kumar, V., and Agarwal, A.K., "Experimental Investigations of Mineral Diesel/Methanol-Fueled Reactivity Controlled Compression Ignition Engine Operated at Variable Engine Loads and Premixed Ratios," *International Journal of Engine Research*1468087420923451, 2020, doi: 10.1177%2F1468087420923451.
43. Wang, Y., Wang, H., Meng, X., Tian, J., Wang, Y., Long, W., Li, S., "Combustion Characteristics of High Pressure Direct-Injected Methanol Ignited By Diesel in a Constant Volume Combustion Chamber," *Fuel* 15;254:115598, 2019, doi: 10.1016/j.fuel.2019.06.006.
44. Dong, Y., Kaario, O., Hassan, G., Ranta, O., Larmi, M., Johansson, B., "High-Pressure Direct Injection of Methanol and Pilot Diesel: A Non-premixed Dual-Fuel Engine Concept," *Fuel* 1;277:117932, 2020, doi: 10.1016/j.fuel.2020.117932.
45. Valera, H., Kumar, D., Singh, A.P., Agarwal, A.K., "Modeling Aspects for Adaptation of Alternative Fuels in IC Engines," In *Simulations and Optical Diagnostics for Internal Combustion Engines* (pp. 9-26). Springer, Singapore, 2020, doi: 10.1007/978-981-15-0335-1_2.
46. Richards, K.J., Senecal, P.K., and Pomraning, E., *CONVERGE 3.0 Manual* (Madison, WI: Convergent Science, 2020).
47. Seiser, R., Pitsch, H., Seshadri, K., Pitz, W.J., and Curran, H.J., *Extinction and Autoignition of n-heptane in Counterflow Configuration* (CA: Lawrence Livermore National Lab, 2000), doi:10.1016/S0082-0784(00)80610-4.
48. Perini, F., Zha, K., Busch, S., Miles, P.C., and Reitz, R.D., "Principal Component Analysis and study of port-induced swirl structures in a light-duty optical diesel engine." Sandia National Lab.(SNL-NM), 2015, doi: 10.4271/2015-01-1696.

Contact Information

Prof. Avinash Kumar Agarwal
Department of Mechanical Engineering
Indian Institute of Technology Kanpur
Kanpur-208016 India
http://home.iitk.ac.in/~akag/
akag@iitk.ac.in
Tel: +91 512 2597982 (Off)
+91 512 2598682 (Res)
Fax: +91 512 2597982, 2597408 (Off)

Acknowledgments

The authors would like to acknowledge the Department of Science and Technology (DST), India, for funding in the procurement of simulation software and high-performance computing machine. The authors also would like to acknowledge Mr. Kamlesh Patel from Convergent Science (India) for their support in model preparation. The authors also would like to acknowledge Dr. Anirudh Gautam from RDSO Lucknow for his help during baseline data collection.

Abbreviations

ICEs - Internal Combustion Engines

IR - Indian Railway

CFD - Computational Fluid Dynamics

CAGR - Compound Annual Growth Rate

RDSO - Research Designs and Standards Organization (A research wing of Indian Railways)

IROAF - Indian Railways Organization for Alternate Fuels

MSW - Municipal Solid Waste

HPDI - High-Pressure Direct Injection

PFI - Port Fuel Injection

FY - Financial Year

3-D - Three Dimensional

1-D - One Dimensional

bTDC - Before Top Dead Centre

TDC - Top Dead Centre

IVO - Inlet Valve Open

IVC - Inlet Valve Close

EVO - Exhaust Valve Open

EVC - Exhaust Valve Close

STL - Stereolithography

RANS - Reynolds Averages Navier-Stokes Equation

RNG - Re-normalization Group

KH - Kelvin-Helmholtz

RT - Rayleigh-Taylor

TKE - Turbulent Kinetic Energy

AMR - Adaptive Mesh Refinement

NTC - No Time Counter

Base Model - Locomotive Engine when fueled with only diesel

M+D Model - Locomotive Engine Model when fueled with methanol and pilot diesel

O_2 - Oxygen

CO - Carbon Monoxide

CO_2 - Carbon Dioxide

CAD - Crank Angle Degree

Appendices:

Appendix A. Instrument/ Software details

- **3-D Convergent Science**
- CONVERGE Studio VERSION 3.0
- Solver: CONVERGE/3.0.12/
- **Tecplot**
- Tecplot 360 EX 2019 R1
- Version 2019.1.0.99403
- **Origin**
- OriginPro 2020b (64-bit)
- Version 9.7.5.184 (Learning Edition)
- **Workstation**
- 128 GB RAM, Ubuntu 18.04.5 LTS (GNU/Linux 4.15.0-130-generic x86_64)

Appendix B. Software Available Options

- **Converge Studio**

FIGURE 14 Converge Studio Interface

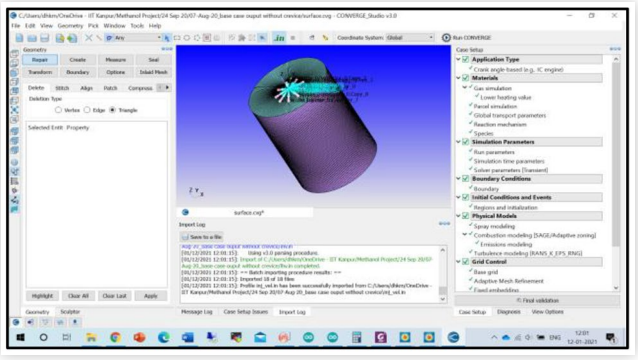

- **Tecplot**

FIGURE 15 Tecplot Interface - 1

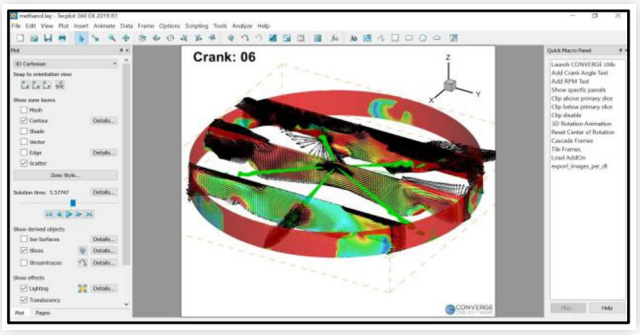

FIGURE 16 Tecplot Interface - 1

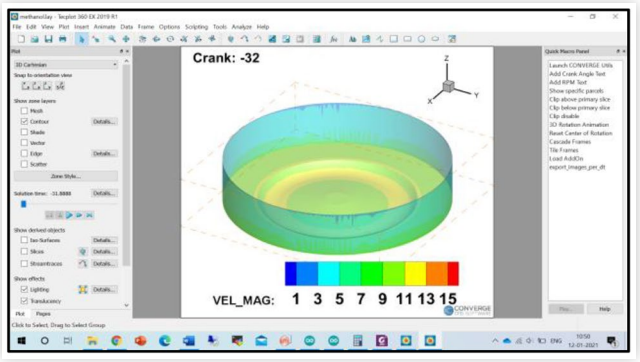

ISSN 0148-7191